Sigma J Eng Nat Sci, Vol. 44, No. 1, pp. 234–251, February, 2026

Sigma Journal of Engineering and Natural Sciences
Web page info: https://sigma.yildiz.edu.tr
DOI: 10.14744/sigma.2026.1980

Research Article

Impact of halloysite clay on the thermal degradation behaviour, kinetics analysis, and pyrolysis product distribution during catalytic pyrolysis of bakelite

Chinmaya KAR[1], Achyut KUMAR PANDA[1], Pabitra MOHAN MAHAPATRA[2,*]

[1]*Veer Surendra Sai University of Technology, Burla, 466001, India*
[2]*Department of Chemistry, Veer Surendra Sai University of Technology, Burla, Odisha, 466001, India*

ARTICLE INFO

Article history
Received: 04 September 2024
Revised: 25 October 2024
Accepted: 08 December 2024

Keywords:
Batch Pyrolysis; Catalytic Pyrolysis; Coats-Redfern Integral Method; Discarded Bakelite; Halloysite Clay

ABSTRACT

This study is used to explore the effect of a clay catalyst, like Halloysite, on the pyrolysis of Bakelite, showing the different issues of waste bakelite and providing an eco-friendly thermal process to convert the discarded Bakelite into valuable products. In this study, the pyrolysis of Bakelite is conducted to set the backbone of the study. Then, based on the pyrolysis of Bakelite, the catalytic pyrolysis of Bakelite with Halloysite clay is conducted to compare the pyrolysis kinetics and product yields for reactor design. The kinetic analysis is completed by using TGA data and Coats–Redfern modeling from 150–450 °C. The thermodynamic parameters are calculated by the Eyring equation from the TGA data. The TGA data of Bakelite and its blend with the different concentrations (2.5, 5, 7.5, and 10 wt%) of Halloysite clay were obtained at a heating rate of 20 °C/min over the temperature range of 30 to 1000 °C. The batch pyrolysis of the Bakelite in the presence of Halloysite clay is conducted at the optimum pyrolysis temperature for the pyrolysis of Bakelite. The pyrolytic oils produced are analyzed by Fourier transform infrared spectroscopy (FTIR) and gas chromatography–mass spectrometry (GC-MS). The weight loss at a heating rate of 20 °C/min increases from 56.49% to 62.57% with the addition of 5 wt% Halloysite clay. The degradation of Bakelite without Halloysite clay follows a 1.5th-order kinetic mechanism with an activation energy of 81.088 kJ/mol and an Arrhenius constant of 4.39×10^{12} min^{-1}. However, with 5 wt% Halloysite clay, the activation energy decreases to 77.883 kJ/mol and the Arrhenius constant drops to 2.08×10^{12} min^{-1}, without changing the kinetic mechanism. The thermodynamic parameters, such as the changes in enthalpy and Gibbs free energy for the thermal degradation of Bakelite, decrease with the addition of Halloysite clay. The addition of 5% Halloysite clay to Bakelite increases the condensable products from 39.12% to 41.25%, while the gas fraction decreases from 30.36% to 29.51% and the residue from 30.52% to 29.24%. FTIR and GC-MS support the presence of alkanes, cycloalkanes, alkenes, cycloalkenes, aromatics, and oxygenated species in the pyrolytic oils. These results highlight that the addition of Halloysite clay with Bakelite during thermal conversion alters the kinetic analysis, improves the product yields, and varies the composition of the pyrolytic oil. The novelty of this study lies in demonstrating the catalytic effect of Halloysite clay on thermal degradation, kinetics, and product distribution for optimal reactor design.

Cite this article as: Kar C, Kumar Panda A, Mohan Mahapatra P. Impact of halloysite clay on the thermal degradation behaviour, kinetics analysis, and pyrolysis product distribution during catalytic pyrolysis of bakelite. Sigma J Eng Nat Sci 2026;44(1):234–251.

***Corresponding author.**
*E-mail address: pabitra.mahapatra3@gmail.com; pmmahapatra_phdchem@vssut.ac.in

This paper was recommended for publication in revised form by Regional Editor Ahmet Selim Dalkilic

INTRODUCTION

The polymer and its composite-based materials are widely used for manufacturing heat-resistant components in the automotive and aerospace industries [1]. The use of polymers has grown due to their low density, poor heat and electrical conductivity, high strength, flexibility, and low cost [2]. About 1.75×10^5 tons/annual of Bakelite are used in over 15,000 products [3]. The synthetic Bakelite is used widely in the manufacture of electronics, glassware, chemicals, metals, polymers, mobile cases, kitchenware, containers, and pipe stems [4]. The global Bakelite market is expected to increase from USD 3.51 billion in 2024 to USD 4.22 billion by 2029, with a CAGR of over 3.5% [5]. The widespread use of Bakelite increases the volume of discarded Bakelite. The Bakelite waste production in India was 8×10^4 tons in 2020, and it is expected to increase to 7 million tons by 2050 [6]. The vast waste of Bakelite causes a negative impact on the environment and human beings. So, bakelite waste is essential to reduce. The microplastics produced from waste plastic cause a major threat to aquatic life [7]. The disposal of waste Bakelite in landfills or the burning of waste Bakelite contaminates water, soil, and air with harmful substances such as methanol, formaldehyde, and asbestos. The cross-linked structure of thermosetting plastic Bakelite provides heat resistance, which complicates recycling [3]. So, developing eco-friendly disposal methods for waste bakelite remains challenging for valorisation, including plastic fuel production in the ongoing research.

To date, researchers are working on new technologies and methods to mitigate Bakelite waste. Mohan et al. used discarded bakelite as a reusable component in concrete beam fabrication [4]. Murali and Sambath mixed waste Bakelite into concrete and used it for solid block manufacturing [3]. Surendranath and Ramana used discarded bakelite as an alternative to conventional aggregates in concrete [6]. Nowadays, many researchers are working on alternative recycling technologies such as thermal and catalytic pyrolysis, gasification, and plasma arc gasification [8]. Dhunna et al. used the waste bakelite as a carbon source in ironmaking [9]. Horikawa et al. carbonised the phenol-formaldehyde resin by using ethylene glycol, 1,6-hexanediol, and polyethylene glycol [10]. Chen et al. synthesized nitrogen-doped mesoporous carbon with 11.64% nitrogen and a 2D hexagonal structure by carbonizing phenolic resin with melamine [11].

Pyrolysis is an efficient, cost-effective method for converting carbon-rich waste into fuels and energy [12]. Pyrolysis is a tertiary recycling process that reduces high molecular weight polymers into smaller molecules in an oxygen-free atmosphere, according to ASTM D5033-00 [13]. This method operates at 300–900°C, converting plastic waste into liquid hydrocarbons, char, and gas. By generating higher-quality liquid hydrocarbons at lower temperatures and with shorter reaction periods, catalytic pyrolysis performs better than thermal pyrolysis and copyrolysis [8]. Xu et al. synthesized carbon aerogels by pyrolyzing phenolic resin gels with $ZnCl_2$ [14]. Wang et al. obtained char residues of 62.9% and 60.5% from pure phenol-formaldehyde resin, and 71.9% and 68.4% from boron carbide-modified PF resin at 700°C and 1000°C, respectively [15].

Research has produced phenolic-rich oils and chemicals from PF resins via pyrolysis, co-pyrolysis, and catalytic pyrolysis [12]. Bennett and Payne examined the volatile organic compounds released during the thermal disintegration of phenolic resin under varied pyrolysis conditions, identifying phenol as the primary product, along with benzene, methylbenzene, 1,4-dimethylbenzene, 1,2-dimethylbenzene, 1,3,5-trimethylbenzene, 2-methylphenol, 4-methylphenol, 2,6-dimethylphenol, 2,4-dimethylphenol, 2,4,6-trimethylphenol, 9H-xanthene, and phenanthrene. They also quantified permanent gases like CO, CO_2, CH_4, and H_2O, excluding hydrogen. Lower heating rates led to more complete decomposition with fewer secondary reactions, while higher rates preserved larger VOC fragments. Faster heating at 20,000°C per second produced more volatile organic compounds and less CO_2 than slower heating at 20°C per minute, though the residue composition remained consistent [16]. Xu et al. synthesized aromatic amines with 14.2% carbon content and 57.6% selectivity from phenol-formaldehyde resins using an HZSM-5-3 zeolite catalyst at 650°C. Adding lignin increased the yield of aromatic amines by 32.2% and achieved 11.8% carbon content at a 1:1 lignin-to-PF resin ratio [17]. Wong et al. performed batch pyrolysis of resole-type phenol-formaldehyde resin from 320 K to 1290 K, resulting in a 39.2% mass loss. They produced three product types: water below 800 K, phenolic derivatives from 500 to 850 K, and permanent gases (H_2, CH_4, CO, CO_2) above 800 K. Aromatics formed between 700 and 850 K, while C_2–C_4 hydrocarbons peaked at 1000 K [18]. Xu et al. showed that pyrolyzing PF resin with calcium hydroxide enhanced thermal decomposition and cracking, increasing monophenol yield. At 650°C and 5% calcium hydroxide, the process produced a phenolic-rich oil with 9.1% aromatic hydrocarbons, 82.8% phenols, and a 33.7% carbon yield. Pyrolyzing the residue at 800°C produced a CaO/char catalyst that reduced bio-oil oxygen content from 14.4% to 2.4% during soybean oil pyrolysis [19]. However, to improve the quality and yield of phenolic-rich oil from waste Bakelite using an optimized reactor, it is need to study the thermal degradation with and without a catalyst, various co-feedstocks, pyrolysis kinetics, and product analysis.

Many studies have been proposed by many researchers regarding the kinetics and mechanisms of bakelite.

Jiang et al. explore the kinetics of the pyrolysis of PF using non-isothermal thermogravimetry at heating rates of 5–20 K/min from 363 to 1100 K. They suggested that the thermal degradation of Bakelite is conducted in three stages. The activation energy, Arrhenius factor, and integral form for the first stage are 222.73 kJ/mol, 1.19×10^9 min^{-1}, and $g(\alpha) = (1-\alpha)^{-3}$; for the second stage they are 271.70 kJ/mol, 4.02×10^6 min^{-1}, and $g(\alpha) = (1-\alpha)^{-1}$; and for the third

stage they are 305.14 kJ/mol, 3.60×10^7 min^{-1}, and $g(\alpha) = 1 + (2/3)\alpha - (1+\alpha)^2/^3$, respectively [20]. Jiang et al. conducted infrared spectroscopy of PF resin pyrolysis from 450 to 750°C. Their research showed that CO and CO_2 arise from methylene group oxidation, with PF resin decomposition driven by methylene scission. However, methylene radicals react with smaller molecules to form volatile compounds like ethylene and methanol. PF resin gradually converts into amorphous carbon as temperature increases through pyrolysis and polycyclic reactions [21].

Catalytic pyrolysis technology progress is limited by the lack of effective, affordable catalysts. Therefore, research on improved catalysts is important to increase the catalytic efficiency and reduce the cost of the catalyst, for commercially producing renewable fuels and chemicals through catalytic pyrolysis [12]. The effective catalytic pyrolysis of waste plastic depends upon the selection of a suitable catalyst [8]. The clay catalysts are widely used due to strong adsorption and surface activity [12]. Clay catalysts have a layered structure, with silica tetrahedra and hydrated alumina octahedra linked by covalent and van der Waals forces [22]. Halloysite (Hal) clay, a cost-effective dioctahedral 1:1 alumosilicate ($Al_2Si_2O_5(OH)_4{\cdot}nH_2O$), is chemically similar to kaolinite. This clay contains internal gibbsite (Al-OH) sheets, external siloxane (Si-O-Si) groups, and a monolayer of water between layers. The hydrated halloysite-(10 Å) has a single water layer between its layers, while dehydrated halloysite-(7 Å) forms by removing interlayer water through mild heating or vacuum.

The spherical or plate-like shape of Halloysite clay depends on its origin [23]. The researcher explores the use of different clay catalysts like bentonite, montmorillonite, kaolin, and synthetic hydrotalcite. However, little research has been completed on the use of Halloysite clay. Cai et al. evaluated the catalytic performance of bentonite, montmorillonite, kaolin, and synthetic hydrotalcite in pyrolyzing mixed plastics (PE: PP: PS = 40:20:20:20) for fuel and energy recovery at a 1:10 ratio. The catalyst, like hydrotalcite, increased oil yield and reduced wax. Bentonite increased the gas production, montmorillonite increased the oil production, and kaolin promoted wax generation. Montmorillonite achieved the highest oil yield (71.0%), kaolin produced the most gasoline-range hydrocarbons, and bentonite nanoclay yielded the most diesel-range hydrocarbons. Clay catalysts increased hydrocarbons (methane, ethane, ethene, propene, butane) and reduced CO_2 levels. The study shows that during the catalytic pyrolysis of mixed plastic waste, the moderate acidity of clay catalysts is essential for increasing oil production and gasoline and diesel range fuels. Mechanistic analysis revealed that radicals from plastic breakdown strongly influence the pyrolysis process [12]. Panda and Singh used a batch reactor to fracture waste polypropylene thermally and catalytically at 400–550°C. At 500°C, they obtained the maximum liquid yield (82.85%). Adding kaolin catalyst reduced reaction time and increased production, achieving an 87.5% oil yield at a 1:3 kaolin-to-plastic ratio and 500°C, with oil resembling petroleum fuels [24].

Kanattukara et al. investigated the effect of HNT on the production of pyrolytic oil from HDPE, LLDPE, and PP through catalytic pyrolysis. The HNT catalyst reduced the pyrolysis temperature from 470°C to 450°C and enhanced the yield of liquid. The liquid and gas yields for PP are 66.8% and 32.4%, for HDPE are 51.5% and 37.5%, and for LLDPE are 66.5% and 32.3%, respectively. The HNT catalyst produced a liquid rich in paraffins, naphthenes, olefins, and aromatics, shifting the product distribution toward lighter C_6-C_{10} hydrocarbons, similar to gasoline. The pyrolysis oil with the HNT catalyst contained lighter liquid fractions: 34.2% for PP, 16.0% for LLDPE, and 18.9% for HDPE [13]. Li et al. investigated how poly (butylene adipate-co-terephthalate) (PBAT) is thermally degraded by halloysite nanotubes. Both PBAT and its Halloysite nanotube nanocomposite showed a single-step degradation process. The residual char from PBAT was 0.88%, while the halloysite nanotube/PBAT nanocomposite produced 7.63%, nearly eight times higher. The degradation of both materials released water, alcohols, acids, CO_2, CO, esters, and alkenes [25].

Understanding the chemical kinetics of degradation is crucial for evaluating, designing, and scaling up industrial waste polymer conversion units. The most used technique for examining the kinetics of thermal degradation is thermogravimetric analysis.

There are considerable work has been done to calculate kinetic parameters using the Coats-Redfern model (CR). Ganesha et al. use thermogravimetric analysis and the Coats–Redfern method to investigate the pyrolysis and co-pyrolysis kinetics of mango seed kernel (MSK), mango seed shell (MSS), and PET at heating speeds of 15, 20, and 25°C/min. MSS degraded at higher temperatures than MSK due to its higher cellulose content. The degradation rate depends upon the type of biomass and the PET-to-biomass ratio. Although the reaction order may change depending on the material composition, co-pyrolysis of PET with MSK and MSS increased thermal degradation rates and activation energy. The initial degradation stage has a higher order and lower activation energy than the secondary and tertiary stages. The reaction order varies with raw material composition, ranging from 0.1 to 3 [26]. Arias et al. used thermogravimetric analysis using models such as Friedman, Coats-Redfern, and ASTM E1641 to investigate the effects of particle size (0.3 and 5.0 mm) on waste tire pyrolysis kinetics. Waste tire pyrolysis occurs in two stages between 200 and 520°C, involving plasticizer volatilization and rubber degradation. The larger sizes cause higher kinetic parameters due to heat and mass transfer processes. The activation energy in the Friedman model varied between 40 and 117 kJ/mol for particles of 0.3 mm and between 23 and 119 kJ/mol for particles of 5.0 mm. The activation energy in the Coats-Redfern model varied between 46 and 87 kJ/mol for 0.3 mm and 43 and 124 kJ/mol for 5.0 mm. According

to ASTM E1641, activation energy was 56-60 kJ/mol for both 0.3- and 5.0-mm particles. The reaction order was approximately one in both decomposition zones [27]. Uzun et al. investigated the co-pyrolysis behavior and kinetics of blends of walnut shell, polypropylene, and low-density polyethylene (1:2, 1:1, and 2:1 ratios) using the Arrhenius and Coats–Redfern models and thermogravimetric analysis data at heating rates of 5–50 °C/min. Walnut shell had three devolatilization stages: water removal, hemicellulose/cellulose decomposition, and lignin degradation. Polypropylene and low-density polyethylene decomposed in a single stage with a weight loss of 45% in the active pyrolysis zone. As pyrolysis progressed, activation energy and the Arrhenius factor changed concurrently, indicating a compensating effect. The Arrhenius method gave activation energies of 69.32 kJ/mol for walnut shell, 295.65 kJ/mol for polypropylene, and 254.55 kJ/mol for LDPE, while the Coats-Redfern method yielded 101.58, 333.53, and 316.77 kJ/mol for WS, PP, and LDPE, respectively [28].

Numerous studies have been conducted for converting waste bakelite into valuable products like char, phenolic-rich oils, and chemicals via pyrolysis. However, limited research has focused on the kinetic study and pyrolytic mechanism of bakelite. Several studies have been proposed about the catalytic pyrolysis by using catalysts like kaolin, montmorillonite, bentonite, and halloysite nanotubes to improve yields and efficiency. A lot of work is also completed by using the Coats-Redfern model for the accurate calculation of kinetic parameters. From the above literature review, a research gap is identified, namely, the catalytic batch pyrolysis of Bakelite by using Halloysite clay. This study aims to address these gaps by examining the pyrolytic degradation, kinetic studies using the Coats–Redfern method and thermogravimetry analysis data, thermodynamics analysis by the Eyring equation, and catalytic batch pyrolysis of Bakelite using different concentrations of Halloysite clay. The goal of this study is to improve the valorisation of the waste bakelite by using a suitable clay catalyst. This study offers a novel approach by investigating the catalytic pyrolysis of bakelite using Halloysite clay, a cost-effective material rarely explored for waste management.

MATERIALS AND METHODS

Materials

The discarded electric switches, plugs, and holders collected from the VSSUT electrical maintenance department were used as a source of materials for producing bakelite. The discarded electrical components were first manually broken down into small fragments. These bakelite pieces were then ground into powder using a Philips domestic grinder (model HL7756/00, 750 watts). The ground powder is passed through a No. 18 sieve (Gilson Company, Inc, Model: V8SF#18, ASTM E11 standard) to get a uniform particle size of 1mm. The Hal clay, sourced from Vedayukt India Private Limited, India, has a purity of 98-99% (with Al_2O_3 = 37.079% and SiO_2 = 55.056%). The Halloysite clay sample has the following features: a BET surface area of 7.672 m^2/g, an average pore radius of 7.065 nm, a total pore volume of 0.026 cc/g, and a density ranging from 1.8 to 2.6 g/cm^3. The clay features an irregular plateau shape and a rough surface texture and is utilized as a catalyst.

Methods

Characterization of Bakelite

The proximate analysis is performed by using the different ASTM methods: moisture content (ASTM D 4442), volatile matter (ASTM D 3172), fixed carbon (ASTM D 3177), and ash content (ASTM D 3175). The CHNS elemental analyzer is used for ultimate analysis. The bomb calorimetry is used to calculate the calorific value.

Thermogravimetric Analysis

The study employed a pyrolysis simultaneous thermal analyzer 8000 for Thermogravimetric and Derivative Thermogravimetry evaluation of discarded bakelite and its blends with Hal clay. Samples, each weighing about 9.6 ± 0.25 milligrams, included bakelite and blends with Hal clay at concentrations of 2.5, 5, 7.5, and 10 wt/wt%. The samples are taken in a crucible, and the crucible is subjected to heating under nitrogen flow at 20 ml/min, with temperatures from 30°C to 1000°C and a consistent heating rate of 20°C/min. The thermogravimetry analysis is performed in triplicate to ensure result accuracy.

Batch Pyrolysis and Pyrolysis Oil Analysis

The pyrolysis and catalytic pyrolysis of Bakelite using different concentrations (2.5, 5, 7.5, and 10 wt/wt%) of Halloysite clay are performed in a stainless-steel tube batch reactor with an internal diameter of 37 mm, an exterior diameter of 41 mm, and a length of 145 mm. The reactor, which features a top opening, was filled with 30 grams of sample and securely sealed with nuts and bolts. The batch reactor is heated using an external electric furnace at a heating rate of 20 °C per minute. The reactor temperature was monitored using a Cr-Al: K thermocouple, and the temperature is regulated with an accuracy of ±3.6 °C by a PID controller. The pyrolysis temperature ranges from 300 to 500 °C, revealing that 450 °C is the optimal temperature for bakelite pyrolysis, maximizing the yield of condensable fractions. Therefore, catalytic pyrolysis of the bakelite-Hal clay blend is also performed at 450 °C. The vapors formed are passed through a condenser to condense into liquid and wax. The non-condensable gases are away from the system. The residual solid is collected from the reactor. By comparing the mass of the collected materials to the initial mass of the reactant, the yield of liquid and wax products was evaluated. The percentage yield of the pyrolytic products, including condensable substances and residue, is calculated, and the non-condensable gases are calculated by subtracting from 100%. The batch pyrolysis experiment is

conducted three times for each sample to maintain accuracy and reliability. The FTIR analysis of the pyrolytic oils is performed by using a Bruker Alpha FTIR spectrophotometer (Resolution = 2 cm^{-1} and Spectrum range = 500–4000 cm^{-1}). For GC-MS analysis, a Shimadzu GC-MS QP 2020 NX system with an SH-Rxi-5ms capillary non-polar column (30 m × 0.25 mm ID × 0.25 μm film thickness) was utilized.

The GC-MS analysis is conducted by including the experimental condition: Carrier gas (He): 1.0 mL/min, Injection volume: 1 μL, Temperature program: 35–280 °C at 5 °C/min, and Mass range: 35–650 m/z (NIST 20 library.

Pyrolysis Kinetic Theory

The complexity of pyrolysis makes it difficult to create kinetic models that fully explain the principles underlying thermal breakdown. However, instead of a complete kinetic analysis, average kinetic values can still be used [29]. The thermogravimetry analysis data are used in the Coats-Redfern integral method to calculate the kinetic parameters [30].

The overall rate of pyrolytic degradation of bakelite in the absence and presence of Hal clay (dα/dt) is defined by equation 1.

$$\frac{d\alpha}{dt} = kf(\alpha) \tag{1}$$

Here, f(α) is a function of α, and the value of f(α) varies from model to model, and k is the rate constant [31].

The earlier work suggests that the thermal degradation of Bakelite follows the F_5 order mechanism [32]. Catalysts influence cracking rates [33], allowing variations in reaction order without altering the overall model with the Hal catalyst. Therefore, this study employed the order-based Coats-Redfern model for clarity, as adding other models could complicate the analysis without significant benefits. Equation 2 defines the value of f(α) for the nth-order decomposition reaction.

$$f(\alpha) = (1-\alpha)^n \tag{2} [34]$$

The reaction order (n) is used to describe the pyrolysis model.

The value of the extent of pyrolysis of the sample (α) derived from thermo-gravimetric analysis, and is expressed as: [29]

$$\alpha = \frac{W_i - W_t}{W_i - W_f} \tag{3}$$

Here, W_i = Initial weight of the sample at time t = 0, W_t = Weight of the sample at an intermediate time t, and W_f = Final weight of the sample as time approaches infinity

The relationship between temperature and the rate constant k is described by the Arrhenius equation, provided as:

$$k = A \exp\left(-\frac{Ea}{RT}\right) \tag{4} [35]$$

Ea stands for activation energy, R for universal gas constant, T for absolute temperature, and A for pre-exponential component in equation 4.

From equation (1) and (4)

$$\frac{d\alpha}{dt} = A \exp\left(-\frac{Ea}{RT}\right) f(\alpha)$$
$$\Rightarrow \frac{d\alpha}{f(\alpha)} = A \exp\left(-\frac{Ea}{RT}\right) dt \tag{5}$$

Now integrate the equation (5)

$$g(\alpha) = \int_0^\alpha \frac{d\alpha}{f(\alpha)} = A \int_0^t \exp\left(-\frac{Ea}{RT}\right) dt \tag{6}$$

Now multiply and divide dT with the right side of equation (6)

$$\int_0^\alpha \frac{d\alpha}{f(\alpha)} = A \int_0^t \exp\left(-\frac{Ea}{RT}\right) dt \times \frac{dT}{dT}$$
$$\Rightarrow \int_0^\alpha \frac{d\alpha}{f(\alpha)} = A \int_0^t \exp\left(-\frac{Ea}{RT}\right) \frac{dt}{dT} \times dT \tag{7}$$

For the linear heating program,

Heating rate (β) = dT/dt (8) [36]

From equation (7) and (8)

$$\int_0^\alpha \frac{d\alpha}{f(\alpha)} = A \int_0^T \exp\left(-\frac{Ea}{RT}\right) \frac{1}{\beta} \times dT$$
$$\Rightarrow \int_0^\alpha \frac{d\alpha}{f(\alpha)} = \frac{A}{\beta} \int_0^T \exp\left(-\frac{Ea}{RT}\right) dT \tag{9} [31]$$

The right-hand side of equation (9), though obtaining a precise analytical solution is not possible.

By using Cauchy's rule, the equation (9) becomes

$$\frac{A}{\beta} \int_0^T \exp\left(-\frac{Ea}{RT}\right) dT \cong \frac{ART^2}{\beta Ea}\left(1-\frac{2RT}{Ea}\right)\exp\left(-\frac{Ea}{RT}\right) \tag{10}$$

From equation (9) and (10)

$$\int_0^\alpha \frac{d\alpha}{f(\alpha)} = \frac{ART^2}{\beta Ea}\left(1-\frac{2RT}{Ea}\right)\exp\left(-\frac{Ea}{RT}\right) \tag{11}$$

From equation (2) and (11)

$$\int_0^\alpha \frac{d\alpha}{(1-\alpha)^n} = \frac{ART^2}{\beta Ea}\left(1-\frac{2RT}{Ea}\right)\exp\left(-\frac{Ea}{RT}\right) \tag{12}$$

Since, (2RT/Ea) <<< 1, So, the value of (2RT/Ea) is neglected, and equation (12) becomes

$$\int_0^{\alpha}\frac{d\alpha}{(1-\alpha)^n}\cong\frac{ART^2}{\beta Ea}\exp\left(\frac{-Ea}{RT}\right)$$
$$\Rightarrow\int_0^{\alpha}(1-\alpha)^{(-n)}d\alpha=\frac{ART^2}{\beta Ea}\exp\left(\frac{-Ea}{RT}\right)$$
$$\Rightarrow\left[\frac{(1-\alpha)^{(-n+1)}}{(-n+1)}\times(-1)\right]_0^{\alpha}=\frac{ART^2}{\beta Ea}\exp\left(\frac{-Ea}{RT}\right)$$
$$\Rightarrow\left(\frac{(1-\alpha)^{(-n+1)}}{(-n+1)}\times(-1)\right)-\left(\frac{(1)^{(-n+1)}}{(-n+1)}\times(-1)\right)=\frac{ART^2}{\beta Ea}\exp\left(\frac{-Ea}{RT}\right)$$
$$\Rightarrow\frac{(1-\alpha)^{(1-n)}}{(1-n)}\times(-1)-\frac{(1)^{(1-n)}}{(1-n)}\times(-1)=\frac{ART^2}{\beta Ea}\exp\left(\frac{-Ea}{RT}\right)$$
$$\Rightarrow\frac{(1-\alpha)^{(1-n)}}{(1-n)}\times(-1)+\frac{1}{(1-n)}=\frac{ART^2}{\beta Ea}\exp\left(\frac{-Ea}{RT}\right)$$
$$\Rightarrow\frac{1}{(1-n)}-\frac{(1-\alpha)^{(1-n)}}{(1-n)}=\frac{ART^2}{\beta Ea}\exp\left(\frac{-Ea}{RT}\right)$$
$$\Rightarrow\frac{1-(1-\alpha)^{(1-n)}}{(1-n)}=\frac{ART^2}{\beta Ea}\exp\left(\frac{-Ea}{RT}\right)$$

(13) [30]

Now divide T^2 and apply logarithm on both sides

$$\ln\left\{\frac{1-(1-\alpha)^{(1-n)}}{T^2(1-n)}\right\}=\ln\left\{\frac{AR}{\beta Ea}\exp\left(\frac{-Ea}{RT}\right)\right\}$$
$$\Rightarrow\ln\left\{\frac{1-(1-\alpha)^{(1-n)}}{T^2(1-n)}\right\}=\ln\left(\frac{AR}{\beta Ea}\right)-\frac{Ea}{RT}\quad(14)$$

The equation (14) is validated for n≠1

If n=1, then equation (13) becomes,

$$\int_0^{\alpha}\frac{d\alpha}{(1-\alpha)}=\frac{ART^2}{\beta Ea}\exp\left(\frac{-Ea}{RT}\right)$$
$$\Rightarrow\left[-\ln(1-\alpha)\right]_0^{\alpha}=\frac{ART^2}{\beta Ea}\exp\left(\frac{-Ea}{RT}\right)$$
$$\Rightarrow-\ln(1-\alpha)-(-\ln 1)=\frac{ART^2}{\beta Ea}\exp\left(\frac{-Ea}{RT}\right)$$
$$\Rightarrow-\ln(1-\alpha)=\frac{ART^2}{\beta Ea}\exp\left(\frac{-Ea}{RT}\right)\quad(15)$$

Now divide by T^2 and apply logarithm on both sides of equation (15)

$$\ln\left(\frac{-\ln(1-\alpha)}{T^2}\right)=\ln\left(\frac{AR}{\beta Ea}\right)-\frac{Ea}{RT}\quad(16)$$

The Coats-Redfern model equations, given as equations (14) and (16), are employed for calculating kinetic parameters [34]. The Coats-Redfern model kinetic equations used in model-fitting methods are tabulated in Table 1.

By plotting ln [g(α)/T^2] versus 1/T graph, the Y-intercept will be ln [(AR)/(βEa)] and the slope will be – (Ea/R) allowing to determine the values Ea and A respectively [37]. The reaction order for the thermal degradation of bakelite with

Table 1. Coats-Redfern kinetic equation used in model-fitting methods

Method	Kinetic Equations	Plot
CR	(i) $n\neq1$, $\ln\left[\frac{1-(1-\alpha)^{1-n}}{T^2(1-n)}\right]=\ln\left(\frac{AR}{\beta Ea}\right)-\frac{Ea}{RT}$	$\ln\left[\frac{g(\alpha)}{T^2}\right]$ Versus $\frac{1}{T}$
	(ii) $n=1$, $\ln\left[\frac{-\ln(1-\alpha)}{T^2}\right]=\ln\left(\frac{AR}{\beta Ea}\right)-\frac{Ea}{RT}$	

Table 2. Value of f(α) and g(α)

Reaction mechanism	Symbols	f(α)	g(α)
One-half order	$F_{0.5}$	$(1-\alpha)^{1/2}$	$2(1-\alpha)^{1/2}$
First order	F_1	$(1-\alpha)$	$-\ln(1-\alpha)$
Three-halves order	$F_{1.5}$	$(1-\alpha)^{3/2}$	$-2[1-(1-\alpha)^{-(1/2)}]$
Second order	F_2	$(1-\alpha)^2$	$-[1-(1-\alpha)^{-1}]$
Five-halves order	$F_{2.5}$	$(1-\alpha)^{5/2}$	$-(2/3)[1-(1-\alpha)^{-(3/2)}]$
Third order	F_3	$(1-\alpha)^3$	$-(1/2)[1-(1-\alpha)^{-2}]$
Seven-halves order	$F_{3.5}$	$(1-\alpha)^{7/2}$	$-(2/5)[1-(1-\alpha)^{-(5/2)}]$
Fourth-order	F_4	$(1-\alpha)^4$	$-(1/3)[1-(1-\alpha)^{-3}]$
Nine-halves order	$F_{4.5}$	$(1-\alpha)^{9/2}$	$-(2/7)[1-(1-\alpha)^{-(7/2)}]$
Fifth order	F_5	$(1-\alpha)^5$	$-(1/4)[1-(1-\alpha)^{-4}]$
Eleven-halves order	$F_{5.5}$	$(1-\alpha)^{11/2}$	$-(2/9)[1-(1-\alpha)^{-(9/2)}]$
Sixth order	F_6	$(1-\alpha)^6$	$-(1/5)[1-(1-\alpha)^{-5}]$

or without Hal is shown by the plot with the R^2 value closest to 1. The values of g(α) and f(α) are displayed in Table 2 [31, 35].

The activated complex theory and the Eyring equation are employed to calculate further kinetic parameters of the process, as given by:

$$k = \frac{e\chi k_B T_m}{h} \exp\left(\frac{\Delta S}{R}\right) \exp\left(-\frac{Ea}{RT_m}\right) \quad (17)$$

Where, e = Neper number (2.7183)

χ = Transmission factor which is unity for monomolecular reactions

k_B = Boltzmann constant

T_m = Peak temperature which can be obtained from the DTG plot

h = Planck's constant

ΔS = Change in entropy

From equation (4) and (17)

$$A = \left(\frac{e\chi K_B T_m}{h}\right) \exp\left(\frac{\Delta S}{R}\right) \quad (18)$$

$$\Rightarrow \Delta S = R\ln\left(\frac{Ah}{e\chi K_B T_m}\right) \quad (19)\ [35]$$

We know,

$Ea = \Delta H + RT_m$, Where, ΔH = Change in enthalpy

$$\Rightarrow \Delta H = Ea - RT_m \quad (20)$$

According to the Gibbs–Helmholtz equation

$$\Delta G = \Delta H - T_m \Delta S \quad (21)\ [30]$$

Where, ΔG = Change in Free energy

RESULTS AND DISCUSSION

Characterization of Bakelite

The proximate analysis of bakelite shows volatile compounds at 68.22%, moisture at 3.24%, ash at 6.82%, and fixed carbon at 21.72%. Discarded bakelite can be used as a possible feedstock for pyrolysis because of its high volatile content, and its high fixed carbon content increases the possibility that it will be converted into useful carbonaceous products [32]. However, the moisture content necessitates additional energy for drying, and the relatively high ash content increases both handling and processing costs [38].

The ultimate analysis of bakelite reveals a carbon content of 68.04%, oxygen at 14.78%, and hydrogen at 5.09%. Pyrolytic degradation of Bakelite produces more oxygenated compounds due to the presence of oxygen. Bakelite has zero nitrogen and sulfur content, so no nitrogen- or sulfur-containing compounds are produced [38]. A high amount of carbon and hydrogen produces a higher number of aromatic compounds. This high carbon and hydrogen content causes a higher heating value of Bakelite. With a calorific value of 6610 Cal/g, bakelite is an efficient fuel that can be utilized to maximize combustion temperature in operations involving the use of raw materials [39].

TG-DTG Analysis

In earlier research, the thermal study was conducted at various heating rates (5, 10, 20, 30, and 50°C/min) [32]. According to the ICTAC guidelines [40], heating rates in the 1–20°C/min range are commonly used, as this range provides reliable and reproducible results for TGA/DTG analysis. The moderate heating rate of 20 °C/min is selected for the TG–DTG analysis of the impact of Halloysite clay on the thermal degradation of Bakelite to ensure continuity and comparability with earlier findings at heating rates ranging from 5 to 50 °C/min. Figure 1 presents the TG–DTG curve for the thermal degradation of Bakelite in the absence and presence

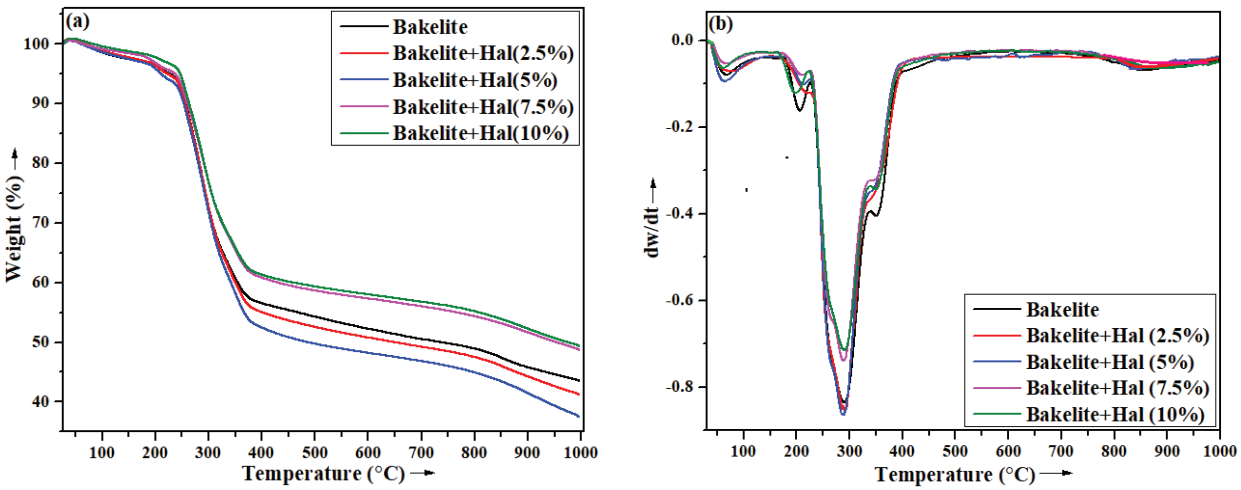

Figure 1. (a) TGA, (b) DTG of bakelite and its blends with Hal clay.

of different concentrations (2.5%, 5%, 7.5%, and 10%) of Hal clay at a heating rate of 20 °C/min.

The temperature affects the extent of the pyrolytic cracking reaction, which changes the quantities of condensable gases, non-condensable gases, and char yield. At a lower temperature, long-chain hydrocarbons are formed, but at higher temperatures, these long hydrocarbons undergo C-C bond cracking to form shorter hydrocarbons. Secondary reactions, which lead to the formation of aromatic compounds, are more prominent at elevated temperatures. Catalytic conditions further enhance the conversion rate at lower temperatures than thermal pyrolysis [8]. The Hal clay catalyst enhances the reaction rate of thermal degradation of Bakelite, resulting in a lower activation energy. The presence of the Hal clay catalyst promotes phenolation, transalkylation, and oxidative coupling, which leads to the formation of a broader range of degradation products [41]. The pyrolysis of Bakelite follows free radical-initiated chain scission, whereas catalytic pyrolysis of Bakelite occurs via a carbocation mechanism. Therefore, the presence of the Halloysite clay catalyst changes the product distribution and composition [12]. The larger compounds begin degrading on the outer surface of the catalyst, but with further degradation, the process occurs in the internal pores, influencing product selectivity. Adding 5% Hal clay catalyst promotes bakelite degradation; however, a higher catalyst/polymer ratio leads to more char formation. Therefore, as Hal clay concentration is increased from 5% to 7.5% and 10%, weight loss decreases, resulting in more residue [8]. However, compared to pyrolysis without the catalyst, weight loss increases when the concentration of Hal clay is decreased from 5% to 2.5%, although it stays lower than when the concentration of Hal clay is 5%. This could be due to an inadequate amount of catalyst for effective degradation. Table 3 shows the initial temperature (T_i), peak temperature (T_m), final temperature (T_f), and percentage weight loss (W) at different stages from Figure 1.

According to Table 3, bakelite loses 56.95% of its total weight when heated at a heating rate of 20°C per minute. When blended with Hal clay at concentrations of 2.5%, 5%, 7.5%, and 10% wt/wt, the weight losses change to 58.9%, 62.57%, 51.45%, and 50.71%, respectively. The 5% concentration proves to be the most effective, leading to the highest weight loss. At a heating rate of 20°C/min, the thermal degradation of discarded bakelite and its blend with Hal clay of varying concentrations takes place in four stages over a temperature range of 30 to 1,000°C, both with and without the Hal clay catalyst. The addition of a 5% Hal clay catalyst accelerates all stages of thermal degradation of Bakelite. Bakelite loses 3.01% in the first stage (30–185°C), while Bakelite with 5% Hal catalyst loses 3.38% in the first stage (30–186°C), mainly due to the loss of adsorbed water and volatile substances. Bakelite loses 2.49% in the second stage (185–231°C), while Bakelite with 5% Hal catalyst loses 2.77% in the second stage (186–230°C), primarily due to phenol derivatives, heavier aromatic species, and water

Table 3. Thermal weight loss profile of bakelite with halloysite clay at different concentrations as a catalyst at various stages

Sample	First stage				Second stage				Third stage				Four stage				Total weight loss (%)
	Ti	Tm	Tf	W	Ti	Tm	Tf	W	Ti	Tm	Tf	W	Ti	Tm	Tf	W	
Bakelite	30	65	185	3.01	185	212	231	2.49	231	290	392	37.70	392	852	1000	13.75	56.95
Bakelite + Hal (2.5%)	30	77	184	2.88	184	220	232	2.60	232	290	395	40.16	395	854	1000	13.26	58.90
Bakelite + Hal (5%)	30	64	186	3.38	186	215	230	2.77	230	289	391	40.89	391	845	1000	15.53	62.57
Bakelite + Hal (7.5%)	30	67	180	2.09	180	214	227	2.31	227	289	390	34.35	390	875	1000	12.70	51.45
Bakelite + Hal (10%)	30	62	172	1.60	172	198	226	1.74	226	289	393	35.12	393	878	1000	12.25	50.71

released during degradation and cross-linking. Bakelite loses 37.70% in the third stage (231–392°C), while Bakelite with 5% Hal catalyst loses 40.89% in the second stage (230–391°C), mainly due to the release of volatiles, water, and unreacted oligomers. Bakelite loses 13.75% in the fourth stage (392–1000°C), while Bakelite with 5% Hal catalyst loses 15.53% in the second stage (391–1000°C), mainly due to the release of volatiles, water, and unreacted oligomers. The weight loss in this stage is primarily due to the release of CO, CO_2, CH_4, methanol, Tar, aromatic hydrogen, benzene, toluene, xylene, phenol, 2,6-xylenol, 2,4-xylenol, and 2,4,6-Trimethylphenol, naphthalene, biphenyl, dibenzofurans, fluorene, phenanthrene, and anthracene. The residue obtained at the end of the thermal degradation process is a mixture of char and major fillers, including SiO_2, Al_2O_3, BaO, CaO, and ZnO [32].

There is no consistent trend in the variation of peak temperature with the addition of different concentrations of Hal clay catalyst to bakelite. Figure 1(b) confirms that the addition of 5% Hal clay results in a decrease in peak temperatures in the first stage (65–64°C), third stage (289–290°C), and fourth stage (852–845°C), while the second stage shows a slight growth in peak temperature from 212°C to 215°C.

Kinetic Analysis Through Model Fitting

Kinetic graphs for the thermal degradation of bakelite, and its blend with Hal clay at 2.5%, 5%, 7.5%, and 10% wt/wt concentrations, were produced using non-isothermal thermogravimetric data and the Coats-Redfern model equations. The kinetic graphs are shown in Figure 2 at a heating rate of 20°C/min.

The activation energy and Arrhenius factor for the thermal degradation of bakelite in the absence and presence of Hal clay catalyst at several concentrations (2.5, 5, 7.5, and 10% wt/wt) are calculated by slope and Y-intercept of kinetic graphs, respectively. Table 4 shows the values of activation energy, Arrhenius factor, and regression factor for several order-based reaction models. The different values of f(α) for various order-based models result in variations in both the slope and the Y-intercept of the kinetic plots. This is because each reaction order model assumes a distinct relationship between conversion (α) and time or temperature, leading to different mathematical expressions f(α). Therefore, the activation energy and Arrhenius factor were calculated from the slope and Y-intercept of these plots and vary depending on the order of the reaction being modeled. The variation of activation energy and Arrhenius factor values proves the need to select the appropriate reaction order for accurately analyzing the thermal degradation kinetics. The best-fit kinetic model provides more reliable kinetic parameters and improves understanding of the degradation mechanisms. The results of activation energy, pre-exponential factor, and correlation coefficient for the thermal degradation of Bakelite in the absence and presence of Hal clay catalyst at different concentrations (2.5, 5, 7.5, and 10 wt%) are listed in Table 4.

Using a variety of kinetic models, including model fitting and model-free (KAS, FWO, STR, FRM, LTA, VYZ, and Kissinger), the non-isothermal degradation of bakelite was investigated in a previous study at heating rates of 5, 10, 20, 30, and 50°C/min in a nitrogen atmosphere. It was discovered to follow an F_5 order-based mechanism with an activation energy of 213 kJ/mol and an Arrhenius factor of 4×10^{16} min.$^{-1}$ [32]. To elaborate, the present study examines how the Coats-Refern method and varying concentrations of Hal clay catalyst affect the kinetic triplets (activation energy, Arrhenius factor, and mechanism) of the thermal degradation of bakelite. From Table 4, it is seen that the value of Ea generally increases with the reaction order for all samples [26]. The pre-exponential factor (A) also rises exponentially with the reaction order, indicating increased reaction complexity at higher orders [31]. Additionally, the R^2 values, which indicate the goodness of fit for the kinetic models, generally increase up to the 1.5th order and then decrease with increasing reaction order, reflecting a decline in model accuracy at higher orders. The value of R^2 for all samples is maximum at the 1.5th order as compared to the other orders. Therefore, the thermal degradation of bakelite with Hal clay catalyst or without Hal clay catalyst of different concentrations follows a 1.5th order mechanism. However, the thermal degradation characteristics of bakelite change with Hal clay concentration, affecting activation energy and Arrhenius factor. The activation energy and Arrhenius factor for the thermal degradation of Bakelite are 81.088 kJ/mol and 4.39×10^{12} min^{-1}, respectively. With 2.5% Hal clay, the activation energy is 79.524 kJ/mol, and the Arrhenius factor is 3.01×10^{12} min^{-1}. With 5% Hal clay, these values are 77.883 kJ/mol and 2.08×10^{12} min^{-1}, respectively. At 7.5% Hal clay, activation energy is 78.471 kJ/mol, and the Arrhenius factor is 2.41×10^{12} min^{-1}. The activation energy increases to 81.732 kJ/mol and the Arrhenius factor to 4.74×10^{12} min^{-1} for the thermal degradation of Bakelite using 10% Hal clay. So, the optimized catalyst for the thermal degradation of Bakelite is 5% Hal clay.

Thermodynamic Parameters

The evaluation of thermodynamic parameters helps determine the energy analysis and feasibility of the pyrolytic process [42]. During forming the activated complex, higher free energy means the reaction is less favorable. Negative change in free energy indicates the reaction is spontaneous, while positive change in free energy indicates it is non-spontaneous and requires extra energy [37]. The enthalpy is the energy required to increase the temperature of a feedstock for pyrolysis until it converts into a product [42]. The positive change in enthalpy confirms an endothermic reaction requiring energy, while a negative change confirms an exothermic reaction that releases energy [37]. The change in free energy shows the amount of heat energy necessary to convert various products, whereas the change

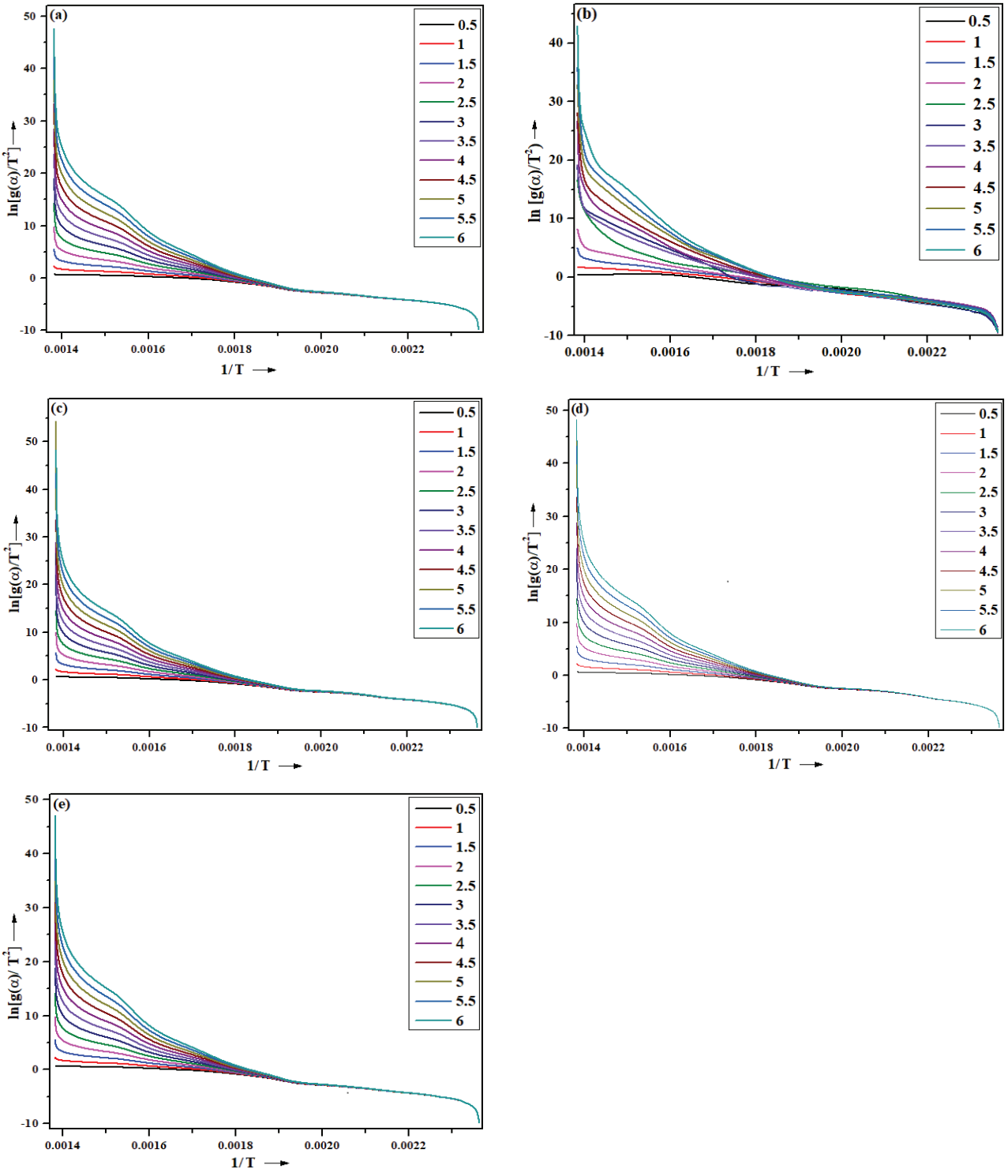

Figure 2. Kinetic plot for pyrolysis of (a) bakelite, (b) bakelite-Hal (2.5%) (c) bakelite-Hal (5%) (d) bakelite-Hal (7.5%), and (e) bakelite-Hal (10%).

in enthalpy value represents the overall energy absorbed by the feedstocks [31]. The entropy change that occurs during thermochemical conversion or combustion defines the thermodynamic complex. A positive change in entropy means the feedstock is more reactive and forms an activated complex faster. In contrast, a negative change indicates the reaction reaches equilibrium quickly and forms a more ordered complex [42]. The values of ΔS, ΔH, and ΔG for bakelite and its mixes with Hal clay at various concentrations (2.5%, 5%, 7.5%, and 10% wt/wt) were computed

Table 4. Outcomes of kinetics analysis of bakelite, and its blends

Order	Bakelite			Bakelite + Hal (2.5%)		
	Ea	A	R2	Ea	A	R2
0.5	58.362	1.08×10^{10}	0.940	59.077	1.20×10^{10}	0.907
1	67.833	1.36×10^{11}	0.974	67.254	1.16×10^{11}	0.977
1.5	81.088	4.39×10^{12}	0.990	79.524	3.01×10^{12}	0.990
2	97.398	3.02×10^{14}	0.979	94.955	1.71×10^{14}	0.977
2.5	115.602	3.26×10^{16}	0.954	124.578	4.68×10^{17}	0.909
3	134.939	4.61×10^{18}	0.928	147.163	1.11×10^{20}	0.909
3.5	154.991	7.66×10^{20}	0.905	168.590	8.58×10^{21}	0.877
4	175.523	1.42×10^{23}	0.885	169.852	4.24×10^{22}	0.874
4.5	196.398	2.83×10^{25}	0.869	188.649	4.71×10^{24}	0.871
5	217.528	5.96×10^{27}	0.855	212.735	2.08×10^{27}	0.860
5.5	238.855	1.31×10^{30}	0.844	226.227	7.09×10^{28}	0.841
6	260.337	2.97×10^{32}	0.835	252.738	4.18×10^{31}	0.834
Order	**Bakelite + Hal (5%)**			**Bakelite + Hal (7.5%)**			**Bakelite + Hal (10%)**		
	Ea	**A**	**R2**	**Ea**	**A**	**R2**	**Ea**	**A**	**R2**
0.5	56.360	$7.02\times1^{0}9$	0.941	56.727	7.66×10^{9}	0.935	59.347	1.30×10^{10}	0.942
1	65.378	7.78×10^{10}	0.976	65.816	8.67×10^{10}	0.972	68.682	1.56×10^{11}	0.976
1.5	77.883	2.08×10^{12}	0.990	78.471	2.41×10^{12}	0.988	81.732	4.74×10^{12}	0.990
2	93.219	1.11×10^{14}	0.975	94.003	1.35×10^{14}	0.975	97.777	3.02×10^{14}	0.977
2.5	110.332	9.12×10^{15}	0.947	111.335	1.18×10^{16}	0.948	115.672	3.00×10^{16}	0.950
3	128.647	9.92×10^{17}	0.915	130.024	1.41×10^{18}	0.915	134.677	3.86×10^{18}	0.922
3.5	147.414	1.19×10^{20}	0.892	148.874	1.73×10^{20}	0.893	154.385	5.83×10^{20}	0.897
4	166.770	1.63×10^{22}	0.870	168.462	2.51×10^{22}	0.872	174.567	9.79×10^{22}	0.876
4.5	186.463	2.41×10^{24}	0.853	188.388	3.93×10^{24}	0.854	195.089	1.77×10^{25}	0.859
5	206.654	3.99×10^{26}	0.835	209.110	7.44×10^{26}	0.835	215.864	3.38×10^{27}	0.844
5.5	226.547	6.11×10^{28}	0.826	228.938	1.12×10^{29}	0.828	236.834	6.74×10^{29}	0.832
6	246.842	$1.02\times1^{03}1$	0.816	249.466	2.00×10^{31}	0.818	257.961	1.39×10^{32}	0.822

using equations 19-21 at a heating rate of 20°C/min. The results of thermodynamic parameters are shown in Table 5.

From Table 5, it is seen that the value of ΔS and ΔH increase, but ΔG decreases as order increases. The non-spontaneity of the reactions across all temperatures is demonstrated by positive ΔG and ΔH values and a negative ΔS [32]. Therefore, the 0.5th, 1st order, 1.5th, and 2nd order based thermal degradation reaction of bakelite and its blends with different concentrations (2.5, 5, 7.5, and 10 %wt/wt) show a non-spontaneous reaction, while others are not. The thermal degradation reactions, which all have a positive ΔH, are endothermic, and this is consistent across reactions of all orders. The thermal degradation reactions of bakelite and its blends (2.5%, 5%, 7.5%, and 10% wt/wt) for 0.5th, 1st, 1.5th, and 2nd orders show a negative entropy change, indicating the formation of a more ordered system. These reactions reach equilibrium quickly and form a stable complex. In contrast, reactions of other orders are more reactive, forming the activated complex faster and resulting in a less ordered system. For the 1.5th order-based thermal degradation, bakelite shows ΔS, ΔH, and ΔG values of -0.050 $kJK^{-1}mol^{-1}$, 76.415 kJ/mol, and 104.803 kJ/mol, respectively, while for bakelite blended with Hal clay, the values are -0.054 $kJK^{-1}mol^{-1}$, 74.844 kJ/mol, and 105.050 kJ/mol for 2.5% Hal clay; -0.057 $kJK^{-1}mol^{-1}$, 73.210 kJ/mol, and 105.095 kJ/mol for 5% Hal clay; -0.055 $kJK^{-1}mol^{-1}$, 73.873 kJ/mol, and 104.492 kJ/mol for 7.5% Hal clay; and -0.050 $kJK^{-1}mol^{-1}$, 77.059 kJ/mol, and 105.088 kJ/mol for 10% Hal clay, respectively. Among the others, the 5% Hal clay catalyst blend for bakelite's 1.5th order-based thermal degradation offers the benefit of the lowest entropy and enthalpy among the blends, suggesting a more controlled degradation process with less disorder and lower heat absorption. These results are useful to confirm a more stable and efficient thermal degradation process. The change in entropy for the thermal degradation of Bakelite in the presence of Hal clay (5%) is slightly greater, creating more disorder during the process. The lower change in enthalpy leads to more energy-efficient degradation. The

Table 5. Outcomes of thermodynamic parameters of bakelite and its blends

Order	Bakelite			Bakelite +Hal (2.5%)		
	ΔS	ΔH	ΔG	ΔS	ΔH	ΔG
0.5	-0.100	53.681	110.220	-0.099	54.396	110.461
1	-0.079	63.152	107.873	-0.081	62.573	108.009
1.5	-0.050	76.407	104.853	-0.054	74.844	105.050
2	-0.015	92.717	101.365	-0.020	90.274	101.589
2.5	0.024	110.921	97.638	0.046	119.897	94.153
3	0.065	130.258	93.804	0.127	163.909	92.215
3.5	0.107	150.310	89.922	0.091	142.482	91.168
4	0.151	170.842	86.018	0.141	165.172	85.997
4.5	0.195	191.717	82.106	0.180	183.969	82.754
5	0.239	212.847	78.193	0.230	208.054	78.332
5.5	0.284	234.174	74.280	0.260	221.546	75.301
6	0.329	255.656	70.370	0.313	248.057	71.955

Order	Bakelite +Hal (5%)			Bakelite +Hal (7.5%)			Bakelite +Hal (10%)		
	ΔS	ΔH	ΔG	ΔS	ΔH	ΔG	ΔS	ΔH	ΔG
0.5	-0.104	51.697	110.165	-0.103	52.054	110.112	-0.099	54.674	110.264
1	-0.084	60.706	107.935	-0.083	61.144	107.864	-0.078	64.010	107.999
1.5	-0.057	73.210	105.095	-0.055	73.798	104.992	-0.050	77.059	105.088
2	-0.024	88.546	101.830	-0.022	89.331	101.689	-0.015	93.104	101.725
2.5	0.013	105.660	98.351	0.015	106.662	98.167	0.023	111.001	98.136
3	0.052	123.975	94.757	0.055	125.352	94.507	0.063	130.005	94.443
3.5	0.092	142.741	91.154	0.095	144.201	90.882	0.105	149.712	90.705
4	0.133	162.098	87.515	0.136	163.790	87.199	0.148	169.895	86.947
4.5	0.174	181.791	83.870	0.178	183.715	83.510	0.191	190.416	83.181
5	0.217	201.981	80.191	0.222	204.448	79.745	0.235	211.191	79.413
5.5	0.258	221.874	76.579	0.264	224.266	76.130	0.279	232.162	75.647
6	0.301	242.169	72.937	0.307	244.793	72.444	0.323	253.288	71.883

*ΔS = $kJK^{-1}mol^{-1}$, ΔH = kJ/mol, ΔG = kJ/mol

greater change in Gibbs free energy makes the process less spontaneous than pure Bakelite.

Batch Pyrolysis Outcomes and Oil Characterization

The conditions of the process and the type of plastic significantly affect the yields and compositions of the final products [43]. Catalysts also influence product distribution by promoting further cracking of initial fragments into smaller hydrocarbons at their active sites [13]. In the batch pyrolysis of bakelite and its Hal clay-catalyzed variant at 450°C, products such as waxy oil, pure wax, residue, and non-condensable gas were classified. Figures 3 (a) and (b) present the yield versus products and feedstock type versus reaction time, respectively.

Figure 3a shows that the yields of waxy oil, pure wax, gas, and residue during batch pyrolysis of bakelite are 11.73%, 27.39%, 30.52%, and 30.36%, respectively, while during Hal clay (5%) catalyzed pyrolysis, the yields are 16.42%, 24.83%, 29.24%, and 29.24%, respectively. Cai et al. found that using a clay catalyst notably enhances the production of liquid products while decreasing the yields of wax and gas. Additionally, the catalyst effectively inhibits the further conversion of liquid oil into gas [12]. Pyrolysis causes the development of solid residue (char) through condensation. A catalyst increases the ash concentration and H/C ratio of the char without changing its elemental composition. Nevertheless, the buildup of char on the catalyst can lower its active sites, thereby diminishing catalytic performance. The catalyst also enhances the quality and amount of the resultant liquid oil [8]. Viscous and waxy products result from inadequate cracking of plastics into high molecular weight hydrocarbons. Therefore, waxy oil forms rather than pure oil, and pure wax is produced in larger quantities than waxy oil. Catalysts promote polymer cracking by providing a solid surface for the reaction to occur [44]. The external surface of a catalyst is where primary plastic cracking

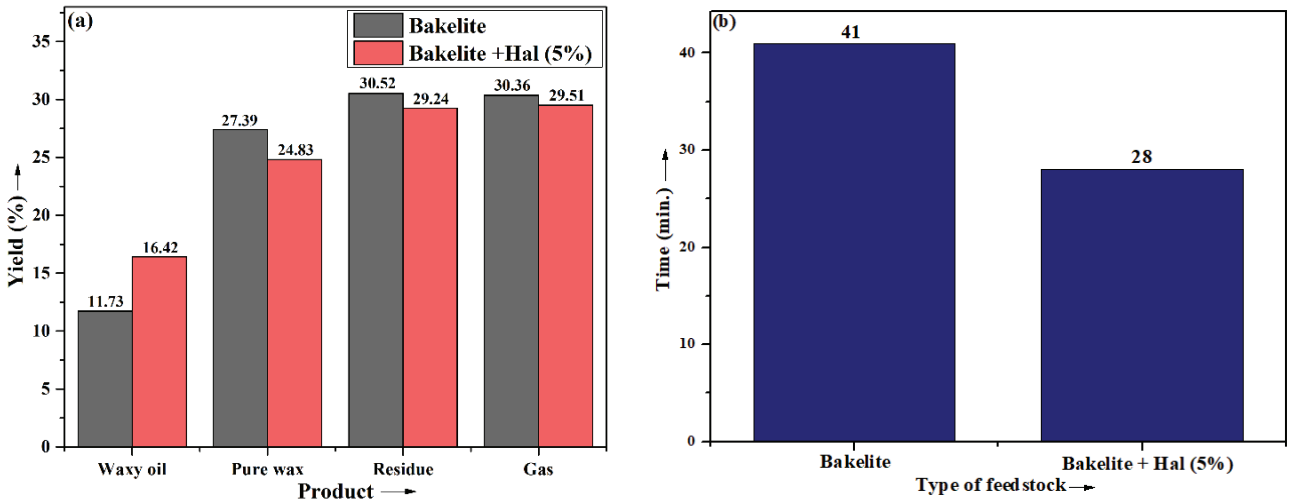

Figure 3. (a) Product versus Yield (b) Types of feedstocks versus Reaction time.

occurs, with subsequent cracking happening inside the pores of the catalyst. So, the surface area and pore volume of the Halloysite clay catalyst have a significant impact on the thermal conversion process, such as pyrolysis. The more the surface area and pore volume, the more the production of gaseous products, and the lower the liquid amount [13]. The thermal degradation of bakelite using Hal clay, which has a smaller surface area and pore volume, produces lower gas and larger liquid yields. Therefore, introducing 5% Hal clay in the pyrolysis of bakelite lowers the formation of pure wax and gas, while enhancing pure oil yields and reducing residue. Figure 3b shows a reduction in the reaction time for bakelite pyrolysis from 41 minutes to 28 minutes with the addition of Hal clay catalyst, as the catalyst accelerates the cracking reactions [8].

The chemical composition of the oils is determined by FTIR and GC-MS analysis. The outcomes of the FTIR analysis for bakelite pyrolysis oils, in the presence and absence of Hal clay, are presented in Figure 4. The FTIR results of the pyrolytic oils have similar functional groups, which confirms that both pyrolytic oils have nearly the same chemical composition. Peaks located at 1015, 1050, and 1106 cm^{-1} suggest the presence of C-C stretching in alkanes. At 2871 and 2968 cm^{-1}, peaks signify the asymmetrical and symmetrical stretching of methyl C-H in alkanes, while the 1453 cm^{-1} peak denotes the bending of both methyl and methylene C-H. The C-H stretching of cycloalkanes is noted at 2968 cm^{-1}. A characteristic peak for C=C stretching in alkenes appears at 1607 cm^{-1}. A peak at 1050 cm^{-1} identifies C-O stretching in alcohols. The two peaks appear at 3209 and 3338 cm^{-1} related to O-H stretching. The peak obtained at 1393 cm^{-1} shows both O-H and C-O bending. The C-O stretch at 1106 cm^{-1} signifies the presence of ether. The peak obtained at 1539 cm^{-1} C=C stretching of aromatic hydrocarbons. The peak obtained at 3665 cm^{-1} indicates O-H stretching of alcohol. The typical peaks at 3549 cm^{-1} and 1393 cm^{-1}, respectively, correspond to O–H and C–O stretching in phenols found in the pyrolytic oil obtained from Bakelite in the presence of the Hal clay (5%) catalyst [45]. These results confirm that both oils have quite similar chemical composition, except for the presence of phenolic content in the pyrolysis oil obtained from Bakelite in the presence of Halloysite clay catalyst. The presence of Phenol as a major compound in the pyrolytic oil is also supported by Bennett and Payne [16]. Wong et al. also reported that phenol derivatives are formed during the batch pyrolysis of resole-type phenol-formaldehyde resin at 500-850K [18]. Xu et al. showed that at 650°C and 5% calcium hydroxide, the pyrolysis of PF produced 82.8% phenols [19]. The FTIR analysis confirmed the presence of alkanes, cycloalkanes, alkenes, alcohols, ethers, and aromatic compounds, and the results are also supported by GC-MS analysis.

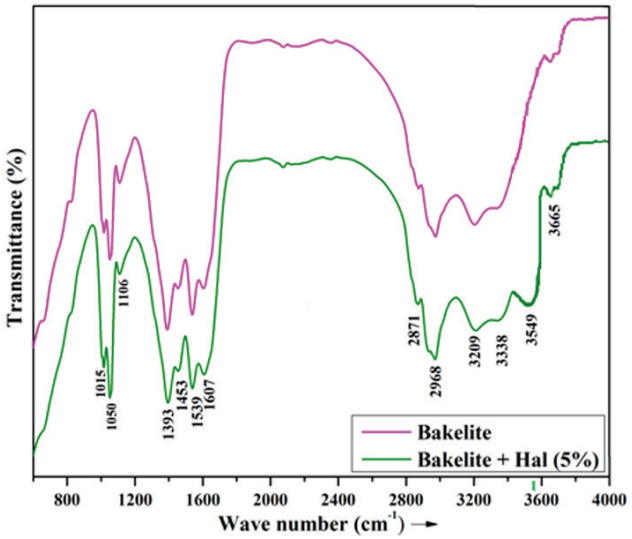

Figure 4. FTIR curve of pyrolytic oils.

The previous work [46] reported that the pyrolytic oil from Bakelite contained compound-like alkane, cycloalkane, alkene, cycloalkene, oxygenated compounds like ester, ketone, alcohol, ether, alcohol, ether, and aromatic compounds. In this work, the oil obtained from Bakelite in the presence of 5% Hal clay catalyst confirms the presence of alkanes, cycloalkanes, alkenes, cycloalkenes, aromatic hydrocarbons, and oxygenated compounds. Wong et al. support the formation of aromatic compounds between 700 and 850 K, while C_2–C_4 hydrocarbons peaked at 1000 K [18]. Xu et al. showed that pyrolyzing PF at 650°C and 5% calcium hydroxide produced 9.1% aromatic hydrocarbons [19]. Table 6 lists different types of compounds present in the pyrolytic oils obtained from the Bakelite in the absence and presence of Halloysite clay (5%).

Research by Ates et al. confirms that catalysts efficiently convert long-chain aliphatic compounds to aromatic ones [47]. Syamsiroa et al., on the other hand, reported that while thermal pyrolysis yields compounds with carbon chains ranging from C_5 to C_{28}, catalysts lead to a higher proportion of lighter oil fractions (C_5-C_{12}) [48]. The GC-MS results (Table 6) show that the presence of Hal clay promotes the production of hydrocarbons, including alkanes, alkenes, cycloalkenes, and aromatic compounds, while reducing the formation of cycloalkane and oxygenated compounds. This shift towards hydrocarbon-rich products results in a more liquid, oil-like consistency, as these hydrocarbons are typically found in the oil fraction of pyrolysis products. On the other hand, the reduction in oxygenated compounds, which often contribute to the formation of solid or

Table 6. GC-MS results of bakelite and bakelite-Hal clay (5%) pyrolysis oils

Compound	Formula	Area (%)	
		Bakelite	Bakelite + Hal (5%)
(i) Alkane		**11.92**	**12.11**
2,3,5-trimethyl hexane	C_9H_{20}	0.20	0.55
3-Ethyl-3-methyl heptane	$C_{10}H_{22}$	0.46	0.85
2,2-Dimethylnonane	$C_{11}H_{24}$	-----	0.78
2,3-Dimethylnonane	$C_{11}H_{24}$	-----	0.81
3,7-dimethyl decane	$C_{12}H_{26}$	0.10	0.25
3-Ethylundecane	$C_{12}H_{26}$	-----	3.15
5-Butyl nonane	$C_{13}H_{28}$	3.40	-----
Tridecane	$C_{13}H_{28}$	-----	0.97
5,5-Diethylpentadecane	$C_{19}H_{40}$	0.82	-----
2-Methylnonadecane	$C_{20}H_{42}$	-----	2.80
2,3-Dimethylnonadecane	$C_{21}H_{44}$	-----	1.95
2,6,10,14,18-Pentamethyl nonadecane	$C_{24}H_{50}$	2.90	-----
Tetracosane	$C_{24}H_{50}$	1.01	-----
11-Methyltricosane	$C_{24}H_{50}$	0.97	-----
2-Methylhentriacontane	$C_{32}H_{66}$	2.06	-----
(ii) Cycloalkane		**2.13**	**1.85**
1,2-Dimethylcyclohexane	$C_{10}H_{18}$	-----	1.30
1,2,3-Trimethylcyclododecane	$C_{12}H_{24}$	-----	0.40
ϒ-Elemene	$C_{15}H_{24}$	1.01	0.15
1,3,5-Triphenyl cyclohexane	$C_{24}H_{24}$	1.12	-----
(iii) Alkene		**7.65**	**7.82**
1,4-Nonadiene	C_9H_{14}	-----	0.45
2,3-Nonadiene	C_9H_{14}	-----	2.50
2,5,6-Trimethyl-1,3,6-heptatriene	$C_{10}H_{16}$	1.30	1.42
2,5-Dimethyl-3-methylene-1,5-heptadiene	$C_{10}H_{16}$	0.62	0.75
2,6-Dimethyl-1,6-octadiene	$C_{10}H_{18}$	2.42	-----
2,3,6-Trimethyl-1,5-heptadiene	$C_{10}H_{18}$	1.36	1.40
2,6-Dimethyl-2,6-octadiene	$C_{10}H_{18}$	0.89	-----
1,3-Undecadiene	$C_{11}H_{20}$	-----	0.95

Table 6. GC-MS results of bakelite and bakelite-Hal clay (5%) pyrolysis oils (continued)

Compound	Formula	Area (%)	
		Bakelite	**Bakelite + Hal (5%)**
1,3-Tridecadiene	$C_{13}H_{24}$	-----	0.35
3-Octadecene	$C_{18}H_{36}$	0.50	-----
Squalene	$C_{30}H_{50}$	0.56	-----
(iv) Cycloalkene		**54.26**	**54.64**
Bicyclo [4.2.0] octa-1,3,5-triene	C_8H_8	6.30	6.51
2,4-Cyclooctadiene	C_8H_{12}	-----	1.23
1,5-Cyclooctadiene	C_8H_{12}	-----	2.50
2,5-Cyclononadiene	C_9H_{12}	-----	1.29
1,3-Cyclononadiene	C_9H_{12}	-----	1.32
D-Limonene	$C_{10}H_{16}$	47.84	41.79
1-Methyl-4-(1-methylethyl) 1,3-cyclohexadiene	$C_{10}H_{16}$	0.12	-----
(v) Aromatic hydrocarbon		**14.74**	**16.76**
Toluene	C_7H_8	1.92	2.1
o-Xylene	C_8H_{10}	-----	2.85
1,2-Dimethylbenzene	C_8H_{10}	-----	2.85
p-Xylene	C_8H_{10}	1.75	1.99
1,3-Dimethylbenzene	C_8H_{10}	-----	1.34
Ethylbenzene	C_8H_{10}	2.83	3.01
α-Methyl Styrene	C_9H_{10}	2.75	-----
Mesitylene	C_9H_{12}	0.84	-----
Propyl benzene	C_9H_{12}	0.80	0.95
Benzene, 1,2,4-trimethyl	C_9H_{12}	-----	0.62
1-Methyl-4-(1-methylethenyl) benzene	$C_{10}H_{12}$	0.91	-----
p-Cymene	$C_{10}H_{14}$	2.51	-----
Biphenyl	$C_{12}H_{10}$	-----	1.05
1,2,3-Trimethylindene	$C_{12}H_{14}$	0.43	-----
(vi) Oxygenate compound		**9.30**	**6.82**
Phenol	C_6H_6O	-----	1.15
2-Methyl phenol	C_7H_8O	-----	1.02
p-Cresol	C_7H_8O	-----	0.55
Benzofuran	C_8H_6O	-----	0.62
2,4-Dimethyl phenol	$C_8H_{10}O$	-----	1.15
1,9-Nonanediol	$C_9H_{20}O_2$	1.00	0.22
Dibenzofuran	$C_{12}H_8O$	-----	0.35
1-Acetoxymethyl-3-isopropenyl-2-methyl cyclopentane	$C_{12}H_{20}O_2$	0.49	0.68
3-(1-Methylhept-1-enyl)-5-methyl-2,5-dihydrofuran-2-one	$C_{13}H_{20}O_2$	0.36	0.15
11-Methyldodecanol	$C_{13}H_{28}O$	0.30	0.11
2-Benzyl-p-cresol	$C_{14}H_{14}O$	-----	0.38
Valeric acid, 2,7-dimethyl oct-7-en-5-yn-4-yl ester	$C_{15}H_{24}O_2$	1.24	-----
2-Ethyl-2-methyl-tri decanol	$C_{16}H_{34}O$	0.53	-----
5,9,13-Trimethyl-4,8,12-tetradecatrien-1-ol	$C_{17}H_{30}O$	0.69	0.32
Methyl palmitate	$C_{17}H_{34}O_2$	1.50	-----
6,9-Octadecadiynoic acid, methyl ester	$C_{19}H_{30}O_2$	0.23	0.12
3-Tridecanoyl cyclo hexen-4-ol-1-one	$C_{19}H_{32}O_3$	1.01	-----
11,14-Eicosadienoic acid, methyl ester	$C_{21}H_{38}O_2$	0.58	-----
Methyl 13,16-docosadienoate	$C_{23}H_{42}O_2$	0.50	-----
1,3-Propanediol, docosyl ethyl ether	$C_{27}H_{56}O_2$	0.87	-----

semi-solid residues like wax, leads to a decrease in the wax content. These results also suggest that Hal clay acts as a catalyst, enhancing the conversion of bakelite into lighter, more volatile hydrocarbon molecules that remain in the oil phase, thereby producing a higher yield of pure oil and a lower yield of wax.

CONCLUSION

This study explores the catalytic pyrolysis of bakelite with varying concentrations of Halloysite clay, demonstrating its significant impact on enhancing pyrolysis kinetics, thermodynamic parameters, product yields, and selectivity toward valuable chemical compounds. The maximum weight loss (62.57%) of bakelite takes place due to the addition of 5 wt/wt % halloysite clay. The degradation process of bakelite using 5 wt/wt % halloysite clay is characterized by a 1.5th order mechanism, with an activation energy of 77.883 kJ/mol and an Arrhenius factor of 2.08×10^{12} min^{-1}. The change in entropy, change in enthalpy, and change in energy values for 1.5th order based thermal degradation of blended bakelite with halloysite clay (5%) are -0.057kJ$K^{-1}mol^{-1}$,73.210kJ/mol, and 105.095 kJ/mol, respectively. In the halloysite clay (5%) catalyzed pyrolysis of bakelite, the yields of condensable products (oil + wax), gas, and residue are 41.25%, 29.51%, and 29.24%, respectively. Fourier transform infrared spectroscopy and gas chromatography-mass spectrometry analysis confirmed that the pyrolysis oil from bakelite with a 5% halloysite clay blend contains alkanes, cycloalkanes, alkenes, alcohols, ethers, phenols, and aromatic chemicals. These results signify the impact of Halloysite clay during the catalytic pyrolysis of Bakelite on reducing activation energy and enhancing yields and quality of valuable products. This study shows that using Halloysite clay in the catalytic pyrolysis of Bakelite improves the kinetics, product yields, and chemical composition for sustainable and scalable industrial applications.

ACKNOWLEDGEMENTS

We express our acknowledgement to TEQIP-III, VSSUT, Burla, for allowing us to use the instrumental facilities available for this research work.

AUTHORSHIP CONTRIBUTIONS

Authors equally contributed to this work.

DATA AVAILABILITY STATEMENT

The authors confirm that the data that supports the findings of this study are available within the article. Raw data that support the finding of this study are available from the corresponding author, upon reasonable request.

CONFLICT OF INTEREST

The author declared no potential conflicts of interest with respect to the research, authorship, and/or publication of this article.

ETHICS

There are no ethical issues with the publication of this manuscript.

STATEMENT ON THE USE OF ARTIFICIAL INTELLIGENCE

Artificial intelligence was not used in the preparation of the article.

REFERENCES

[1] Colak OU, Cakır Y. Genetic algorithm optimization method for parameter estimation in the modeling of storage modulus of thermoplastics. Sigma J Eng Nat Sci 2019;37:981–988.

[2] Cankaya N. Synthesis, characterization, and thermal properties of new oxoethyl acrylate-containing polymer. Sigma J Eng Nat Sci 2020;38:281–288.

[3] Murali K, Sambath K. Transformation of waste bakelite into concrete and solid blocks. IOSR J Mech Civ Eng 2020;17:31–34.

[4] Chakrawarthi RM, Nagaraju TV, Avudaiappan S, Awolusi T, Roco-Videla Á, Azab M, et al. Performance of recycled bakelite plastic waste as eco-friendly aggregate in the concrete beams. Case Stud Constr Mater 2023;18:e02200. [CrossRef]

[5] Bakelite market size. Mordor Intelligence. Available at: https://www.mordorintelligence.com/industry-reports/bakelite-market. Accessed Sep 3, 2024.

[6] Surendranath A, Ramana P. Valorization of bakelite plastic waste aimed at auxiliary comprehensive concrete. Constr Build Mater 2022;325:126851. [CrossRef]

[7] Klun B, Rozman U, Ogrizek M, Kalcikova G. The first plastic produced, but the latest studied in microplastics research. The assessment of leaching, ecotoxicity and bioadhesion of bakelite microplastics. Environ Pollut 2022;307:119454. [CrossRef]

[8] Miandad R, Barakat M, Aburiazaiza AS, Rehan M, Nizami A. Catalytic pyrolysis of plastic waste. A review. Process Saf Environ Prot 2016;102:822–838. [CrossRef]

[9] Dhunna R, Khanna R, Mansuri I, Sahajwalla V. Recycling waste bakelite as an alternative carbon resource for ironmaking applications. ISIJ Int 2014;54:613–619. [CrossRef]

[10] Horikawa T, Ogawa K, Mizuno K, Hayashi J, Muroyama K. Preparation and characterization of the carbonized material of phenol–formaldehyde resin with addition of various organic substances. Carbon 2003;41:465–472. [CrossRef]

[11] Chen H, Zhou M, Wang Z, Zhao S, Guan S. Rich nitrogen-doped ordered mesoporous phenolic resin-based carbon for supercapacitors. Electrochim Acta 2014;148:187–194. [CrossRef]

[12] Cai W, Kumar R, Zheng Y, Zhu Z, Wong JW, Zhao J. Exploring the potential of clay catalysts in catalytic pyrolysis of mixed plastic waste for fuel and energy recovery. Heliyon 2023;9:e23140. [CrossRef]

[13] Kanattukara BV, Singh G, Sarkar P, Chopra A, Singh D, Mondal S, et al, Ramakumar SSV. Catalyst-mediated pyrolysis of waste plastics. Tuning yield, composition, and nature of pyrolysis oil. Environ Sci Pollut Res 2023;30:64994–65010. [CrossRef]

[14] Xu Z, Wang J, Hu Z, Geng R, Gan L. Structure evolutions and high electrochemical performances of carbon aerogels prepared from the pyrolysis of phenolic resin gels containing ZnCl2. Electrochim Acta 2016;231:601–608. [CrossRef]

[15] Wang J, Jiang H, Jiang N. Study on the pyrolysis of phenol-formaldehyde (PF) resin and modified PF resin. Environ Sci Pollut Res 2009;496:136–142. [CrossRef]

[16] Bennett A, Payne D, Court R. Quantitative pyrolytic and elemental analysis of a phenolic resin. 51st AIAA Aerospace Sciences Meeting Including the New Horizons Forum and Aerospace Exposition 2013. 51st AIAA Aerospace Sciences Meeting including the New Horizons Forum and Aerospace Exposition.

[17] Xu L, He Z, Zhang H, Wu S, Dong C, Fang Z. Production of aromatic amines via catalytic co-pyrolysis of lignin and phenol-formaldehyde resins with ammonia over commercial HZSM-5 zeolites. Bioresour Technol 2020;320:124252. [CrossRef]

[18] Wong HW, Peck J, Bonomi RE, Assif J, Panerai F, Reinisch G, Lachaud J, Mansour NN. Quantitative determination of species production from phenol-formaldehyde resin pyrolysis. Polym Degrad Stab 2015;112:122–131. [CrossRef]

[19] Xu L, Zhong Q, Dong Q, Zhang L, Fang Z. Co-production of phenolic oil and CaO/char deoxidation catalyst via catalytic fast pyrolysis of phenol-formaldehyde resin with Ca(OH)2. J Anal Appl Pyrolysis 2019;142:104663. [CrossRef]

[20] Jiang H, Wang J, Wu S, Wang B, Wang Z. Pyrolysis kinetics of phenol–formaldehyde resin by non-isothermal thermogravimetry. Carbon 2009;48:352–358. [CrossRef]

[21] Jiang H, Wang J, Wu S, Yuan Z, Hu Z, Wu R, Liu Q. The pyrolysis mechanism of phenol formaldehyde resin. Polym Degrad Stab 2012;97:1527–1533. [CrossRef]

[22] Parida S, Panda AK. Surface activation of calcium bentonite by acid treatment. Int J Res Chem Environ 2017;54–60.

[23] Sadjadi S. Halloysite nanoclay for the development of heterogeneous catalysts. New York: Elsevier; 2020. p. 275–303. [CrossRef]

[24] Panda AK, Singh RK. Experimental optimization of process for the thermo-catalytic degradation of waste polypropylene to liquid fuel. Adv Energy Eng 2013;1:74–84. [CrossRef]

[25] Li X, Cai Z, Wang X, Zhang Z, Tan D, Xie L, Suna H, Zhong G. The combined effect of absorption and catalysis of halloysite nanotubes during the thermal degradation of PBAT nanocomposites. Appl Clay Sci 2020;196:105762. [CrossRef]

[26] Ganeshan G, Shadangi KP, Mohanty K. Degradation kinetic study of pyrolysis and co-pyrolysis of biomass with polyethylene terephthalate (PET) using Coats–Redfern method. J Therm Anal Calorim 2017;131:1803–1816. [CrossRef]

[27] Arias AMR, Moreno-Pirajan JC, Giraldo L. Kinetic study of waste tire pyrolysis using thermogravimetric analysis. ACS Omega 2022;7:16298–16305. [CrossRef]

[28] Uzun BB, Yaman E. Pyrolysis kinetics of walnut shell and waste polyolefins using thermogravimetric analysis. J Energy Inst 2016;90:825–837. [CrossRef]

[29] Kantarelis E, Yang W, Blasiak W, Forsgren C, Zabaniotou A. Thermochemical treatment of E-waste from small household appliances using highly pre-heated nitrogen. Thermogravimetric investigation and pyrolysis kinetics. Appl Energy 2010;88:922–929. [CrossRef]

[30] Vlaev LT, Markovska I, Lyubchev L. Non-isothermal kinetics of pyrolysis of rice husk. Thermochim Acta 2003;406:1–7. [CrossRef]

[31] Mahapatra PM, Kumar S, Panda AK. Synergy, kinetics, and thermodynamics analysis in the valorization of waste bakelite through co-pyrolysis with HDPE. Cleaner Eng Technol 2023;13:100601. [CrossRef]

[32] Mahapatra PM, Panda AK, Ahmed S, Kumar S. Pyrolysis kinetics and thermodynamics of discarded bakelite. Korean J Chem Eng 2023;40:1380–1388. [CrossRef]

[33] Gebre SH, Sendeku MG, Bahri M. Recent trends in the pyrolysis of non-degradable waste plastics. Chem Open 2021;10:1202–1226. [CrossRef]

[34] Sun J, Wang W, Liu Z, Ma Q, Zhao C, Ma C. Kinetic study of the pyrolysis of waste printed circuit boards subject to conventional and microwave heating. Energies 2012;5:3295–3306. [CrossRef]

[35] Vlaev LT, Nikolova MM, Gospodinov GG. Study on the kinetics of non-isothermal dehydration of alkaline earth metal selenites. Monatshefte Für Chemie Chem Mon 2005;136:1553–1566. [CrossRef]

[36] Coats AW, Redfern JP. Kinetic parameters from thermogravimetric data. Nature 1964;201:68–69. [CrossRef]

[37] Ferfari O, Belaadi A, Bourchak M, Ghernaout D, Ajaj RM, Chai BX. Thermal decomposition of Syagrus romanzoffiana palm fibers. Thermodynamic and kinetic studies using the Coats-Redfern method. Renew Energy 2024;231. [CrossRef]

[38] Mahapatra PM, Panda AK. Co-pyrolytic recycling of bakelite and polymethyl methacrylate. Kinetic, synergistic, and thermodynamic analysis. Chem Select 2024;9. [CrossRef]

[39] Mahapatra PM, Kumar S, Mishra P, Panda AK. Effect of different thermoplastics on the thermal degradation behavior, kinetics, and thermodynamics of discarded bakelite. Environ Sci Pollut Res 2023;31:38788–38800. [CrossRef]

[40] Vyazovkin S, Chrissafis K, Di Lorenzo ML, Koga N, Pijolat M, Roduit B, Sbirrazzuoli N, Sunol JJ. ICTAC kinetics committee recommendations for collecting experimental thermal analysis data for kinetic computations. Thermochim Acta 2014;590:1–23. [CrossRef]

[41] Kasar P, Ahmaruzzaman M. Studies on catalytic co-pyrolysis of bakelite and refineries residual fuel oil using ZSM-5 catalyst to produce lighter fuel oil. J Sci Ind Res Preprint. Available at: https://www.academia.edu/116926541/Studies_on_catalytic_co_pyrolysis_of_bakelite_and_refineries_residual_fuel_oil_using_ZSM_5_catalyst_to_produce_lighter_fuel_oil Accessed on Jan 26, 2025.

[42] Mahapatra PM, Mishra PC, Kumar S, Mishra P, Panda AK. Investigation of synergetic, kinetics, thermodynamics, and batch pyrolysis of polypropylene-bakelite co-pyrolysis. Results Eng 2023;21:101720. [CrossRef]

[43] Colantonio S, Cafiero L, De Angelis D, Ippolito NM, Tuffi R, Ciprioti SV. Thermal and catalytic pyrolysis of a synthetic mixture representative of packaging plastics residue. Front Chem Sci Eng 2019;14:288–303. [CrossRef]

[44] Panda AK, Singh RK. Catalytic performances of kaoline and silica-alumina in the thermal degradation of polypropylene. J Fuel Chem Technol 2011;39:198–202. [CrossRef]

[45] Sharma YR. Elementary organic spectroscopy. Ram Namgar, New Delhi: S Chand Publishing; 2007.

[46] Mahapatra PM, Pradhan D, Kumar S, Panda AK. Isothermal pyrolysis of discarded bakelite. Kinetics analysis and batch pyrolysis studies. Circul Econ 2024;100102. [CrossRef]

[47] Ateş F, Miskolczi N, Borsodi N. Comparision of real waste (MSW and MPW) pyrolysis in batch reactor over different catalysts. Part I: Product yields, gas and pyrolysis oil properties. Bioresour Technol 2013;133:443–454. [CrossRef]

[48] Syamsiro M, Saptoadi H, Norsujianto T, Noviasri P, Cheng S, Alimuddin Z, Yoshikawa K. Fuel oil production from municipal plastic wastes in sequential pyrolysis and catalytic reforming reactors. Energy Proced 2014;47:180–188. [CrossRef]